PROCEEDINGS, Thirty-Third Workshop on Geothermal Reservoir Engineering
Stanford University, Stanford, California, January 28-30, 2008
SGP-TR-185

SEISMIC MONITORING OF EGS TESTS AT THE COSO GEOTHERMAL AREA, CALIFORNIA, USING ACCURATE MEQ LOCATIONS AND FULL MOMENT TENSORS

Gillian R. Foulger[1], Bruce R. Julian[2], Francis C. Monastero[3]

[1]Dept. Earth Sciences, University of Durham, Science Laboratories, South Rd., Durham, DH1 3LE, U.K., e-mail: g.r.foulger@durham.ac.uk

[2]U.S. Geological Survey, 345 Middlefield Rd., Menlo Park, CA 94306, e-mail: julian@usgs.gov

[3]Geothermal Program Office, U.S. Navy, China Lake, CA 93555-6001, e-mail: francis.monastero@navy.mil

ABSTRACT

We studied high-resolution relative locations and full moment tensors of microearthquakes (MEQs) occurring before, during and following Enhanced Geothermal Systems (EGS) experiments in two wells at the Coso geothermal area, California. The objective was to map new fractures, determine the mode and sense of failure, and characterize the stress cycle associated with injection. New software developed for this work combines waveform cross-correlation measurement of arrival times with relative relocation methods, and assesses confidence regions for moment tensors derived using linear-programming methods. For moment tensor determination we also developed a convenient Graphical User Interface (GUI), to streamline the work.

We used data from the U.S. Navy's permanent network of three-component digital borehole seismometers and from 14 portable three-component digital instruments. The latter supplemented the permanent network during injection experiments in well 34A-9 in 2004 and well 34-9RD2 in 2005. In the experiment in well 34A-9, the co-injection earthquakes were more numerous, smaller, more explosive and had more horizontal motion, compared with the pre-injection earthquakes. In the experiment in well 34-9RD2 the relocated hypocenters reveal a well-defined planar structure, 700 m long and 600 m high in the depth range 0.8 to 1.4 km below sea level, striking N 20˚ E and dipping at 75˚ to the WNW. The moment tensors show that it corresponds to a mode I (opening) crack. For both wells, the perturbed stress state near the bottom of the well persisted for at least two months following the injection.

HIGH-RESOLUTION HYPOCENTERS

MEQs are traditionally located independently and individually by inverting measured seismic-wave arrival times picked either automatically or by an operator. This method, even with the benefit of an excellent seismic wave-speed model (Foulger and Julian, 2004) and highly skilled arrival-time picking, yields hypocentral locations with errors of many tens of meters relative to one another.

Relative location accuracy can be improved with the use of modern programs that locate large clusters of MEQs simultaneously (Waldhauser and Ellsworth, 2000). The absolute location of the cluster is little improved by this technique, but the error in the locations of the individual MEQs relative to others in the cluster is much reduced. We applied this method, via the computer program **hypocc** (Julian, in preparation-b), to MEQs induced in EGS injection experiments at the Coso geothermal area.

We improved the locations still further by picking seismic-wave arrival times automatically using waveform cross-correlation. For this we developed the program **toonpics** (Julian, in preparation-c). We repicked the MEQs using this method and relatively relocated them again. The resulting locations thus benefited from both refinements and provided the ultimate relative location accuracy currently available.

SEISMIC MOMENT TENSORS

Many earthquakes from geothermal areas have non-double-couple mechanisms (Julian et al., 1998; Miller et al., 1998). These are thought to result from the involvement of fluids in the source process. Simply put, earthquake failure in geothermal areas involves not only shear movement on faults, but also opening and closure of cavities, probably as a result of the flow of abundant, hot, high-pressure fluids (Julian and Foulger, 2004).

Earthquake source mechanisms are traditionally

obtained by plotting *P*-phase polarity data, measured from seismograms, on a map of the focal sphere and analyzing the distribution of compressions and dilations. A "double-couple" (DC) interpretation, appropriate for pure shear faulting, implies that the compressions and dilatations can be separated by orthogonal planes (great circles on the map). If the source is not assumed to be solely shear, then the lines separating the compressional and dilatational fields are not generally great circles, but ellipses. Under some circumstances they may be small circles but this need not be the case.

Non-DC source mechanisms are specified by moment tensors, which involve two more free parameters than DCs, and require more advanced data processing for their determination. We use compressional and shear seismic-wave amplitudes in addition to polarity data, to obtain general descriptions of the motions at the source.

Amplitudes alone are subject to severe bias by wave-propagation effects such as focusing and attenuation. To counteract this problem we invert seismic-wave amplitude ratios, along with polarities, using a linear-programming algorithm (Julian, 1986; Julian and Foulger, 1996). This combination of data and inversion approach can determine moment tensors for MEQs at least three magnitudes smaller than other methods can.

A useful way to display moment tensors is on the orientation-independent "source-type plot" (Hudson et al., 1989). All DCs lie at the center of this plot. Mechanisms that plot above the center line involve explosive (volume-increase) components and those that plot below have implosive components. The horizontal position on the plot depends on the detailed type of shear involved.

We recently developed a technique to assess uncertainties in derived moment tensors (Julian, 1986; Julian and Foulger, 1996). The linear-programming method finds the moment tensor that best fits a set of observed seismic-wave polarities and amplitude ratios, in the sense of minimizing the L1 norm (the sum of absolute values) of the misfits to the observations ("data residuals"). We extended the method to determine what changes to this best-fit solution can be made while keeping the goodness of fit within a specified range. We formulate this task itself as a linear-programming problem, and solve it efficiently by standard methods.

To use the new method, the user specifies a number of "objective functions", linear combinations of the moment-tensor components that are to be maximized or minimized subject to keeping the L1 norm of the residuals within certain bounds that the user also specifies. Examples of such objective functions include the volume change, the amount of extension or compression in specified directions, and the similarity to particular chosen mechanisms.

Because computing moment tensors is a complex and time-consuming processes, we also developed a convenient Graphics User Interface (GUI) to speed the work (Julian, in preparation-a). Earlier software tools amounted to a bundle of command-line-driven developer scripts, and determining each moment tensor might take several hours. Using the new GUI, determining a moment tensor typically takes ~ 20 minutes. The GUI cannot speed manual picking of the polarities and amplitudes, which must still be done by hand, but elimination of outliers and inversion of the data is greatly streamlined.

APPLICATIONS

Overall goal

We sought to map new fractures, determine the mode and sense of failure, and characterize the stress cycle associated with fluid injections in EGS experiments. We therefore conducted studies of MEQs induced by two Enhanced Geothermal Systems (EGS) experiments in wells at the Coso geothermal area, California. The area is monitored excellently by the U.S. Navy via a high-quality permanent network of three-component digital seismometers, supplemented by 14 portable stations installed at the surface (Figure 1) (Julian et al., 2004).

We calculated high-resolution relative locations and full moment tensors of MEQs occurring before, during and following the fluid injections. Joint interpretation of these two independent sets of results enables reduction of the ambiguity inherent in interpretation of either on its own. The GUI greatly speeded the moment tensor work and made it possible to process much larger sets of MEQs. Analysis of the uncertainties associated with the moment tensors is beginning to give insights into the reliability of different aspects of the results, and to point the way to promising avenues of future work.

Experiment in well 3A4-9, August 2004

Well 34A-9 was originally drilled to a depth of 2,985 m in 1993, and temperatures exceeding 300˚C were encountered–amongst the highest ever recorded in the Coso area. The permeability of the formations drilled was poor, and the well was shut in January 2004. Stimulation was conducted in August 2004 to bring 34A-9 back into service as an injector.

Brine was injected at 127˚C (260˚F) for 1 week at 1200 kg/hr, followed by 71˚C (160˚F) at 960 kg/hr

decreasing to 480 kg/hr for 3 weeks. This induced a vigorous swarm of MEQs (Figures 2 & 3). High-resolution hypocenters were calculated using the new **toonpics** cross-correlation software, coupled with the relative-relocation program **hypocc**. The MEQs were divided into pre-, co- and post-injection periods as follows:

20040601-20040806 – the pre-injection period
20040806-20040813 – the co-injection period
20040813-20041101 – the post-injection period

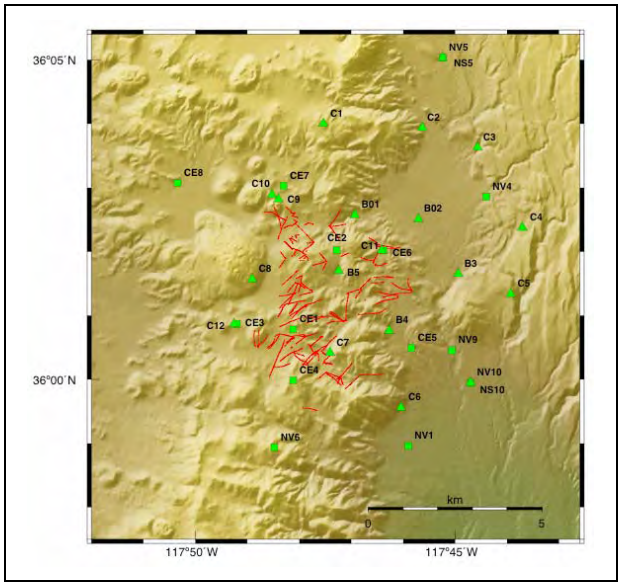

Figure 1: Map showing seismometers at the Coso geothermal area. Red lines: boreholes; squares: permanent seismometers of the Navy network; triangles: portable seismometers.

The results for the co-injection period are shown in Figure 4. Substantial improvement in location clustering, compared with the U.S. Navy catalog, was achieved using **hypocc** (compare left and middle panels of Figure 4).

This is most clearly seen in the vertical sections (lower panels, Figure 4) which are rotated so the view is along the strike of the fault structure imaged. The U.S. Navy locations (lower left panel) show a diffuse cluster only. The middle panel of Figure 4 shows substantially more structure. A NE-striking fault may be distinguished in plan view (top middle panel, Figure 4) and a SE dip is apparent in the vertical section (lower middle panel, Figure 4).

The resolution of this feature is spectacularly improved, however, in the locations obtained using **hypocc** combined with **toonpics** (right panels, Figure 4). The fault plane has a sharp face on the SE side, and strikes N 35˚E and dips 83˚ to the SE.

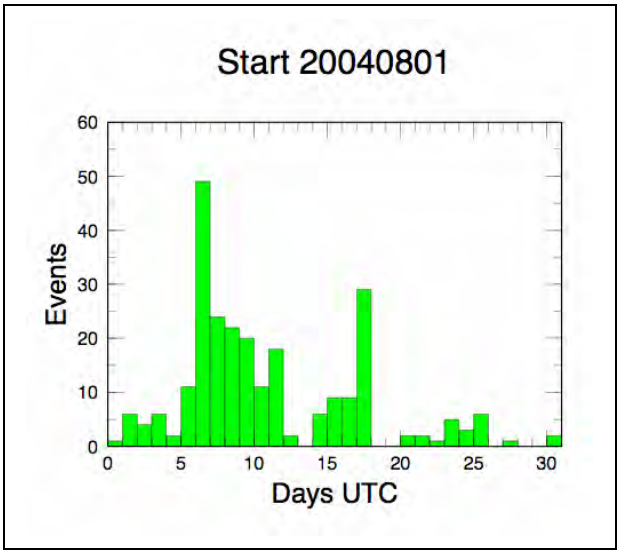

Figure 2. Histogram showing number of microearthquakes per day for August 2004.

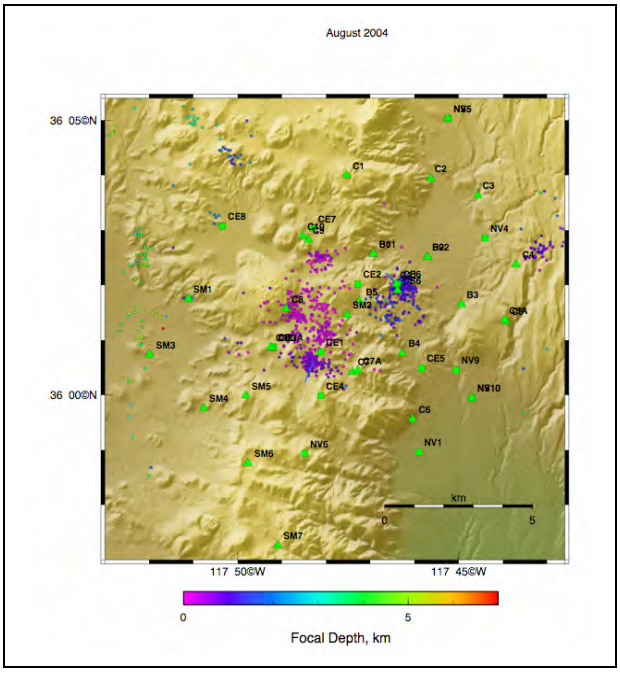

Figure 3. Epicentral map of the Coso geothermal area for August 2004. The shallow cluster of MEQs towards the northeast was induced by injection into well 34A-9.

Significant improvements in focusing of the pre- and post-injection MEQs through application of **toonpics** and **hypocc**, was also achieved.

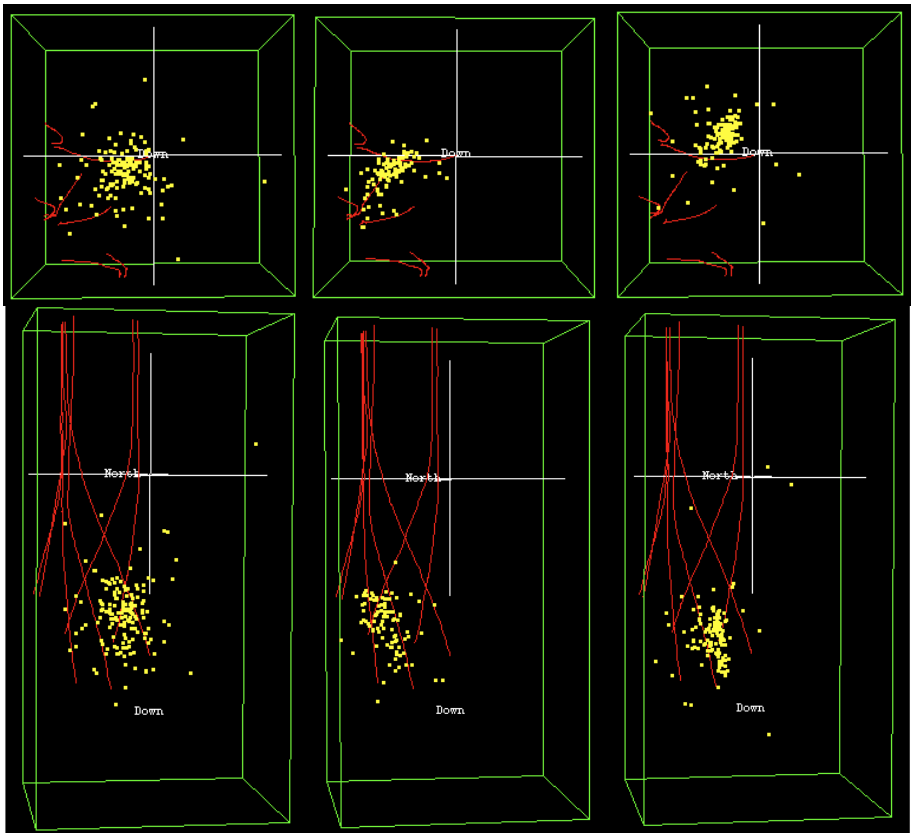

US Navy ***hypocc*** ***toonpics + hypocc***

Figure 4. Locations of MEQs (yellow dots) for the co-injection period. Top row: horizontal maps, bottom row: vertical cross sections rotated so the line of sight is NNE, i.e. aligned along the tectonic strike of local faults. Red lines indicate wells. Left panels: U.S. Navy catalog locations, middle panels: ***hypocc*** *locations, right panels:* ***hypocc+toonpics*** *locations.*

We also computed moment tensors for a large suite of MEQs spanning the pre-, co- and post-injection periods. The largest earthquake for which a good result could be derived had a magnitude of M 2.8. Example results for the co-injection period are shown in Figure 5.

The source types for the MEQs studied vary from double couple (consistent with shear faulting) to having significant crack-opening components. Only a few earthquakes have implosive source types. The pre-, co-, and post-injection earthquakes were all distributed in a broadly similar way in source-type space.

The injection experiment did not induce earthquakes that had very different volumetric components from the background earthquakes unassociated with injection. Nevertheless, if only the largest earthquakes are considered (plotted in red in Figure 5), a clear tendency is evident for the co-injection events to have systematically larger volume increases.

A preliminary analysis of the errors inherent in the moment tensors was conducted, and an example of the results is shown in Figure 5, middle panel. The source-type parameter k (vertically varying on the plot), which measures the volume change in an earthquake, is better determined than the parameter T (horizontally varying), which quantifies the kind of shear. The source-type parameters k and T can be highly correlated, as shown by the elongated shape of the clusters of points.

It is interesting to note that sets of moment tensors from geothermal areas (e.g., Figure 6) often line up in a similar trend to the error envelope indicated by the

set of sub-optimal results. This suggests that the extreme distribution of moment tensor solutions along that trend may be partly error, a factor that needs to be investigated further in future.

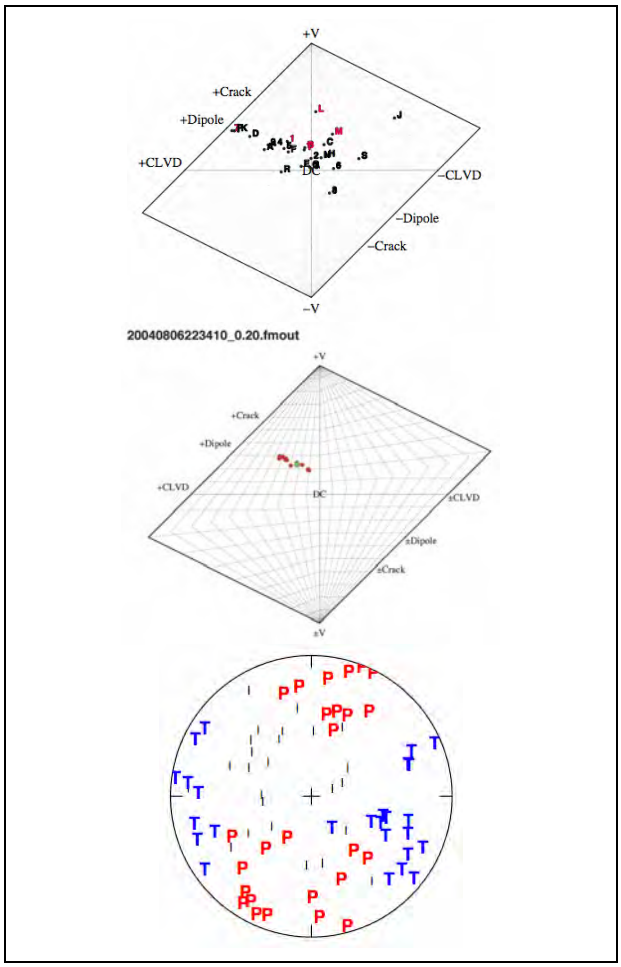

Figure 5. Moment tensor results for the co-injection period. Top: Source-type plot for the 17 moment tensors calculated. The earthquakes are labeled 1-9 and then A-Z to denote their time order. The largest earthquakes are indicated in red. Middle: Error analysis for a single MEQ. The green dot shows the best-fit mechanism and the red dots show 15 extremal mechanisms obtained by maximizing specified linear combinations of the moment-tensor components while keeping the L1 norm of the data residuals below a given limit. Bottom: Equal-area plot of pressure (P), intermediate (I) and tension (T) axes for the same moment-tensor data set.

The source-orientation plots (*e.g.*, bottom panel, Figure 5) show clear variation between the pre-, co- and post-injection earthquake sets. The P-axes of the pre-injection earthquakes tend to be subvertical, and the T-axes are preferentially orientated WNW-ESE, consistent with the general tectonics of the area. The co-injection earthquakes occurred in response to stress of a different orientation, with the P axes preferentially orientated SSW and NNE. There was a particularly notable absence of high-angle P axes in the region of the plot that was most heavily populated for pre-injection earthquakes. The post-injection earthquake source stress orientations comprised a mix of the pre- and co-injection ones, with many earthquakes having high P-axis angles and a few with SSE orientations.

These results together suggest that injection into well 34A-9 modulated the orientation of the local stresses and the mode in which seismic energy was released. Typical background activity was dominated by vertical motion typified by normal faulting. Injection influenced this so that motion had a larger horizontal component and more fracture opening. After injection ceased, the mode of seismic stress release was a combination of the pre- and co-injection styles.

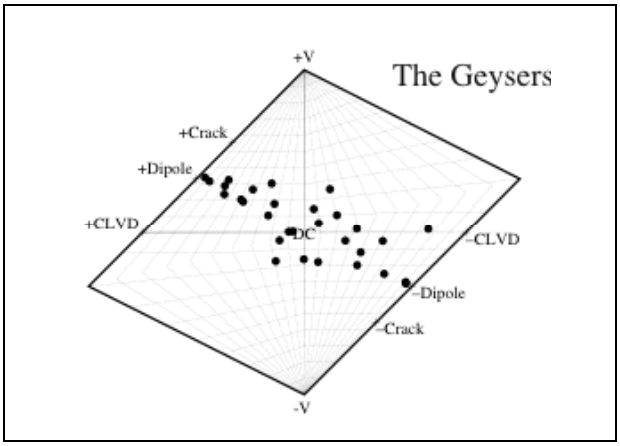

Figure 6. Moment tensors from The Geysers, California, from Ross (1999)

Experiment in Well 34-9RD2, Feb.-March 2005

Well 34-9RD2 was reworked, re-drilled and stimulated February–March 2005. 1st March some large fractures were encountered, resulting in partial mud losses at 2,659 and 2,666 m and total mud losses between 2,672 and 2,677 m. A swarm of MEQs lasting approximately 50 min was induced by this unplanned event. 44 MEQs with magnitudes in the range -0.3 to 2.6 were recorded. Most of the largest occurred in the first 2 min.

We located the MEQs using **hypocc**. Relocation using both **hypocc** and **toonpics** has not yet been performed. As for well 34A-9, improvement in the

clustering of the MEQs was achieved. In order to study variations with time in fracturing associated with the injection test, MEQs that occurred in the neighborhood of well 34-9RD2 for the months preceding and following injection were also processed.

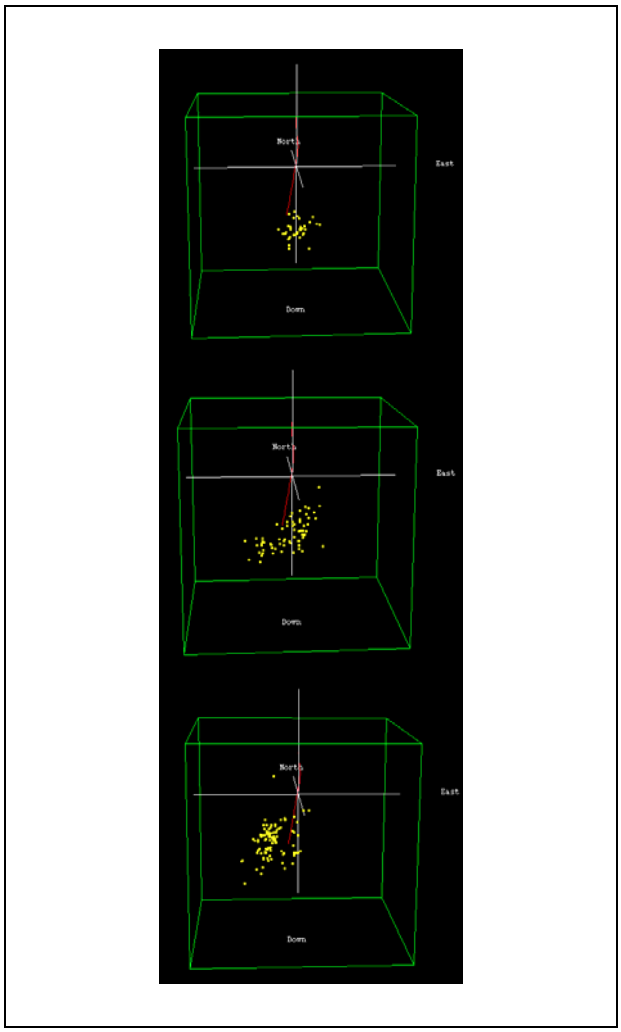

Figure 7. Relatively relocated hypocenters in the neighborhood of well 34-9RD2 from February (upper), March (middle) and April (lower) 2005.

The MEQs for the co-injection period delineate a fault striking at N20˚E, and dipping at 75˚ to WNW (middle panel, Figure 7). They migrated upward and toward the NE with time. Following injection (lower panel, Figure 7) the seismic rate increased, the co-injection swarm location became a "dead zone", and the seismicity migrated out from the co-swarm region, suggesting that the fracture network grew.

Moment tensors were obtained for all the largest MEQs from February–April 2005. Preliminary results for the co-injection MEQs were described by *Julian* (2007). Source-type, and P, T and I axis plots for the pre-swarm month of February are shown in Figure 8.

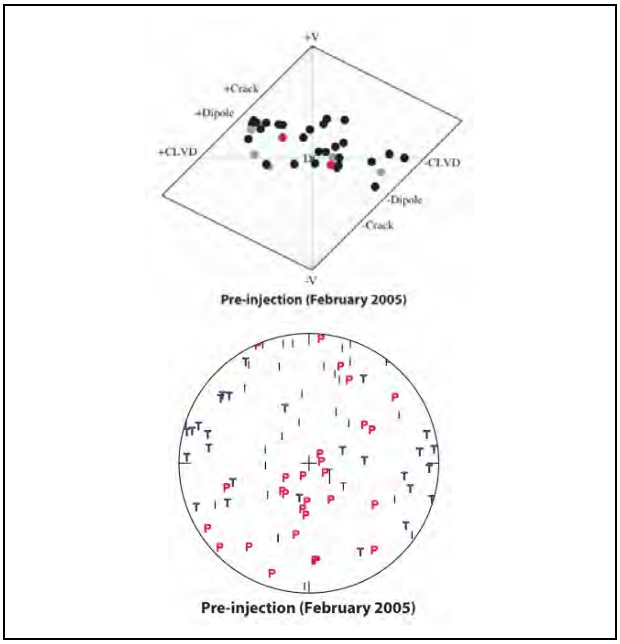

Figure 8. Top: Source-type plots, and bottom: P, T and I axes for pre-injection (February) MEQs.

For the co-injection month of March, 14 good moment tensors were obtained. The results for the co-swarm MEQs were strikingly uniform in mechanism. The fault delineated by the relative relocations is superimposed on the mechanism at top left in Figure 9. The fault bisects the dilatational field on the focal sphere, indicating that the MEQ swarm represented an opening crack (Foulger et al., 2004).

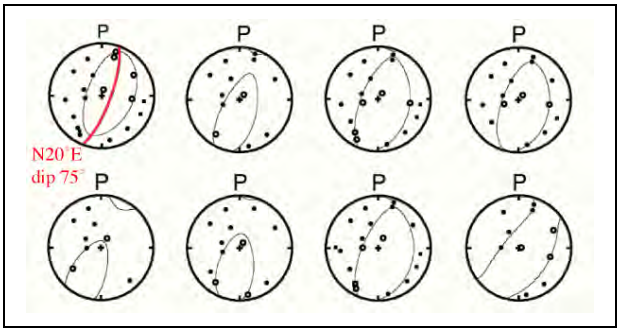

Figure 9. Moment tensor results for 8 co-swarm MEQs. The fault delineated by the relatively relocated hypocenters is superimposed on the moment tensor at top left.

Source-type, and P, T and I axis plots for the post-

swarm month of April are shown in Figure 10. The moment tensors and P, T, and I axes indicate that the mode of stress release in the vicinity of Well 34-9RD2 changed throughout the 3-month EGS cycle. The "volumetric rate" did not decrease on a monthly basis, though MEQs with cavity closing components (implosive components) were largely absent during the co-injection swarm.

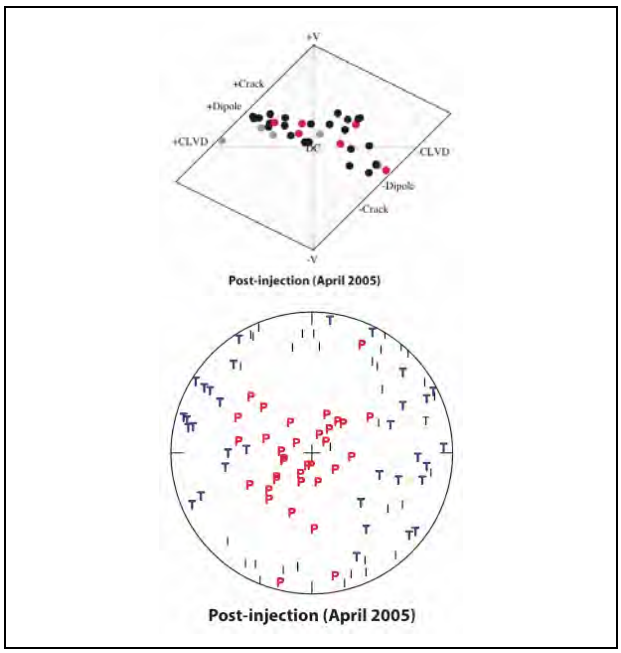

Figure 10. Top: Source-type plots, and bottom: P, T and I axes for post-injection (April) MEQs.

CLOSING REMARKS

The techniques described here represent the state-of-the-art of analysis of MEQs associated with EGS experiments. The techniques are still at a developmental stage, and remain to be fully implemented as routine data processing tools. Nevertheless, they hold much promise for providing the means to know in detail what happens to fluids pumped into the ground down boreholes, and how the rock formation fractures in response.

These techniques potentially have much wider application than injection experiments in geothermal fields only. They may also be applied to the continuous background seismic activity, much of which occurs in response to production. They can thus give information about the response of the bulk reservoir to long-term production. They are also applicable to targets such as production and CO_2 injection in oil reservoirs, injection of hot water into tar sand formations, and monitoring CO_2 sequestration in geologic formations.

REFERENCES

Foulger, G.R. and Julian, B.R., 2004. A powerful tool: Use of time-dependent MEQ tomography for monitoring producing geothermal reservoirs. Geothermal Resources Council Bulletin, 33: 120-126.

Foulger, G.R. et al., 2004. Non-double-couple microearthquakes at Long Valley caldera, California, provide evidence for hydraulic fracturing. Journal of Volcanology and Geothermal Research, 132: 45-71.

Hudson, J.A., Pearce, R.G. and Rogers, R.M., 1989. Source type plot for inversion of the moment tensor. JGR, 94(B1): 765-774.

Julian, B.R., 1986. Analysing seismic-source mechanisms by linear-programming methods. GJRAS, 84: 431-443.

Julian, B.R., in preparation-a. eqmec: A Graphical Tool for Determining Moment Tensors of Microearthquakes, U.S. Geological Survey Open-File Report.

Julian, B.R., in preparation-b. hypocc: A Program for Computing High-Resolution Relative Earthquake Locations, U.S. Geological Survey Open-File Report.

Julian, B.R., in preparation-c. toonpics: A Program for Precise Measurement of Relative Seismic-Wave Arrival Times, U.S. Geological Survey Open-File Report.

Julian, B.R. and Foulger, G.R., 1996. Earthquake mechanisms from linear-programming inversion of seismic-wave amplitude ratios. BSSA, 86(4): 972-980.

Julian, B.R. and Foulger, G.R., 2004. Microearthquake Focal Mechanisms: A Tool for Monitoring Geothermal Systems. Geothermal Resources Council Bulletin, 33: 166-171.

Julian, B.R., Foulger, G.R. and Monastero, F., 2007. Microearthquake moment tensors from the Coso Geothermal area, Thirty-Second Workshop on Geothermal Reservoir Engineering, Stanford University, Stanford, California, pp. SGP-TR-183.

Julian, B.R., Foulger, G.R. and Richards-Dinger, K., 2004. The Coso Geothermal Area: A Laboratory for Advanced MEQ Studies for Geothermal Monitoring, Geothermal Resources Council Annual Meeting. Geothermal Resources Council, Palm Springs.

Julian, B.R., Miller, A.D. and Foulger, G.R., 1998. Non-double-couple earthquakes I. Theory. RG, 36: 525-549.

Miller, A.D., Foulger, G.R. and Julian, B.R., 1998. Non-double-couple earthquakes II.

Observations. Reviews of Geophysics, 36: 551-568.
Ross, A., Foulger, G.R. and Julian, B.R., 1999. Source processes of industrially-induced earthquakes at The Geysers geothermal area, California. Geophysics, 64: 1877-1889.
Waldhauser, F. and Ellsworth, W.L., 2000. A double-difference earthquake location algorithm: Method and application to the northern Hayward Fault, California. BSSA, 90: 1353-1368.